Tellus (2005), 57B, 12–27
Printed in UK. All rights reserved

TELLUS

Model study of the impact of biogenic emission on regional ozone and the effectiveness of emission reduction scenarios over eastern China

By ZHIWEI HAN[1,2]*, HIROMASA UEDA[3] and KAZUHIDE MATSUDA[1], [1]*Acid Deposition and Oxidant Research Center (ADORC), 1182 Sowa, Niigata-shi 950-2144, Japan;* [2]*Institute of Atmospheric Physics, Chinese Academy of Sciences, Beijing 100029, China;* [3]*Disaster Prevention Research Institute, Kyoto University, Uji, Kyoto 611-0011, Japan*

(Manuscript received 5 February 2004; in final form 14 July 2004)

ABSTRACT

The impact of biogenic emission on regional ozone and emission control scenarios has been numerically studied through a series of sensitivity model simulations. A typical episode with elevated ozone over eastern China from 12 to 16 August 2001 was investigated by using a tropospheric chemistry and transport model (TCTM), driven by a non-hydrostatic mesoscale model MM5. The meteorological conditions during this period were characterized by high-pressure systems associated with low wind speeds, high temperatures and clear skies. Afternoon ozone concentrations exceeding 80 parts per billion (ppb) occurred over broad areas of eastern China. There is a generally good agreement between simulation and observation, indicating that the TCTM is able to represent major physical and chemical processes of tropospheric ozone and well reproduce the diurnal and day-to-day variability associated with synoptic conditions. The sensitivity analysis reveals a significant influence of biogenic hydrocarbons on regional ozone. Ozone levels are apparently enhanced by biogenic emission over large areas of eastern China. The largest increase up to 30 ppb in daytime average concentration is found in portions of the middle reaches of the Yangtze River, Yangtze Delta and northeast China. However, the response of ozone to biogenic emission varies spatially, showing more sensitivity in polluted areas than that in clean rural areas. The regimes limited by nitrogen oxides (NO_x) and volatile organic carbon (VOC) in eastern China are further investigated with respect to biogenic emission. Ozone shows a clear tendency to shift from VOC limitation to NO_x limitation as it moves from urban and industrial areas to rural areas. Most of the rural areas in southern China tend to be NO_x limited, whereas most of the northern parts of China appear to be VOC limited. By considering biogenic emission, ozone tends to become more NO_x limited and less VOC limited, both in extent and intensity, over eastern china. Furthermore, some regions have completely shifted from being VOC limited to being NO_x limited.

1. Introduction

China has been experiencing rapid economic expansion over the past two decades. Energy and material consumption during the processes of urbanization and industrialization has brought about a large amount of anthropogenic emission of sulfur dioxide (SO_2), nitrogen oxides (NO_x), volatile organic compounds (VOC) and particulate matter, and has raised serious concerns in society and government.

Although the increasing rate of SO_2 emission had been suppressed in the past decade by implementing emission control strategies and utilizing low-sulfur coal, the emissions of NO_x and VOC show an increasing trend due to expansion of energy consumption and transportation (Elliott et al., 1997; Wang et al., 2000; Streets et al., 2003). As a result, photochemical smog episodes, which are characterized by high levels of ozone and oxidants, often occur in urban and suburban regions (Zhang et al., 1998), as well as wide rural areas of eastern China (Luo et al., 2000; Vincent and Wang, 2001) under favourable meteorological conditions. The surface ozone concentrations have attained almost the same levels as in Europe and America during the summer months (Logan, 1989; McKeen et al., 1991), and in China, pollution by photochemical oxidants has become a difficult problem.

Ozone is a key trace gas, which controls chemical cycles in the troposphere (Levy, 1971). Ozone is produced through a series of nonlinear chemical reactions involving the oxidation of VOC and CO in the presence of sunlight and a catalyser, NO_x (Dodge, 1977; Liu et al., 1987). High ozone values are well known to

*Corresponding author.
e-mail: han@adorc.gr.jp

have adverse effects on human health and vegetation (Chameides et al., 1999). Ozone and its precursors originating locally can be transported over a long distance, leading to an increase in ozone levels on a regional and sometimes even hemispherical scale (Carmichael et al., 1998; Jacob et al., 1999; Lelieveld and Dentener, 2000). Recent studies have revealed an upward trend of ozone concentration in the lower troposphere over East Asia during the last two decades; this was attributed to the increase in anthropogenic emissions in those regions (Akimoto et al., 1996; Oltmans et al., 1998).

Considering the increasing trend of ozone and its potential impact on the environment, much effort has been devoted to the study of the behaviour of ozone in East Asia. These works have focused on the transport and chemical processes of tropospheric ozone under specific weather conditions in different seasons (Liu et al., 1996; Carmichael et al., 1998; Luo et al., 2000; Zhang et al., 2002). During the summer months when photochemical activity and biogenic emission reach their peak, high ozone concentrations are frequently observed over vast areas of eastern China (Zhang et al., 1998; Vincent and Wang, 2001). The elevated ozone level during these episodes may significantly damage human health and the ecosystem, and potentially change the composition of atmospheric chemistry.

Previous studies have revealed the important role of biogenic hydrocarbons in ozone formation over wide rural areas as well as over metropolitan areas (Trainer et al., 1987; Chameides et al., 1988; Roselle et al., 1991). A recent study (Shallcross and Monks, 2000) has also highlighted the role of isoprene, a dominant VOC released by vegetation, in biosphere–climate–chemistry feedback, and indicated the important influence of isoprene on surface and free tropospheric ozone levels as well as on remote atmospheric composition and chemistry.

Approximately 20% or more of the area of eastern China is covered by forest, and large amounts of non-methane hydrocarbons are released from vegetation under intense radiation and high-temperature conditions. In the summer, biogenic emission is expected to reach a maximum under specific synoptic conditions. However, the influence of biogenic emission on chemical species and emission control strategies is still unclear and needs to be investigated in detail.

In this paper, a typical 5-d episode from 12–16 August 2001 was selected and numerically simulated in order to explore a series of issues as follows: the magnitude and distribution of ozone during a typical smog episode and its response to the changes in NO_x and VOC emissions; how and to what extent ozone responds to biogenic emission, and how biogenic emission affects anthropogenic emission control strategies.

In Section 2, the model system and related parameters are introduced. In Section 3, modelled ozone concentrations are presented, comparisons with observational data for meteorological fields, ozone and related species are carried out, and some uncertainties in model simulation and discrepancies in comparison are discussed. Section 4 presents the impact of biogenic emission on the ozone level. Section 5 investigates the ozone sensitivity to changes in anthropogenic NO_x and VOC emissions and reveals how biogenic emission affects the results of emission control scenarios. Conclusions are finally made in Section 6.

2. Model system and input parameters

2.1. Model description

Two models are utilized in this study. One is a mesoscale non-hydrostatic model MM5 (Grell et al., 1994) that has been widely used in simulating mesoscale atmospheric phenomena and boundary layer processes. Another is TCTM (the tropospheric chemistry and transport model), which is used to study the behaviours of chemical species in the troposphere and lower stratosphere (Han et al., 2002). TCTM is a 3-D Eulerian model, developed based on the regional acid deposition model (RADM) (Chang et al., 1987). It includes major processes such as advection, diffusion, gas chemistry and removal processes in the terrain-following sigma coordinate system. An upstream finite-difference advection algorithm with antidiffusive correction (Smolarkiewicz, 1983) is used to solve transport process, ensuring positive values of concentration and fewer computation resources. The turbulent diffusion process is parameterized by using layered horizontal and vertical eddy diffusivity patterns, suggesting different mechanisms of turbulence in the boundary layer and free troposphere (Lei and Chang, 1992a). Dry deposition process of chemical species are calculated by the approach of Lei and Chang (1992b). An updated carbon bond mechanism (CBM-IV) (Gery et al., 1989) with an isoprene mechanism (Carter, 1996) is incorporated into the TCTM to represent gas chemistry; this includes 91 reactions and 37 individual species and is similar to the current version of CBM-IV in community multiscale air quality (CMAQ)/Models-3 (Gipson and Young, 1999). Clear sky photolysis rates are calculated by using the scheme of Madronich (1987). The influence of cloud on photolysis rates is parameterized following the approach of Chang et al. (1987). Aqueous phase chemistry is not taken into account.

2.2. Input parameters for model simulation

The model domain covers eastern China from longitudes 100.0°E to 130°E and latitudes 18°N to 50°N, with the central point at 118.5°E and 34.5°N. Figure 1 illustrates the specific regions and monitoring sites. For MM5, 23 layers stretch unequally from ground to 100 hPa, with a horizontal resolution of 30 km. The reanalysis data sets are derived four times a day with a resolution of $1^\circ \times 1^\circ$ from the National Centers for Environmental Prediction (NCEP) (http://www.ncep.noaa.gov/). TCTM has 17 vertical layers, with about nine layers concentrated in the lowest 2 km of atmosphere in order to resolve boundary layer processes. The model domain of TCTM consists of 79×123 grid cells in east–west and south–north directions with the same horizontal grid size as MM5 on a Lambert conformal map projection.

Fig 1. Specific regions and locations of monitoring sites over eastern China.

The initial concentrations of chemical species are firstly taken as clean background values according to Luo et al. (2000) and brought to the real state through model initialization with actual emissions. Pre-integration was carried out for 3 d, from 9 to 11 August 2001, to minimize the effect of initial conditions and allow ozone and its precursors to build up chemically equilibrated states. The formal integration and analysis period is from 12 to16 August 2001 when high ozone levels occurred over most of the model domain. The lateral boundary conditions are set to clean background values as initial concentrations and are held fixed to reflect any enhancements of species caused by the processes within the domain. Ozone concentrations at the top six altitude levels are valued proportionally to PV (potential vorticity) with 50 ppb per PV in order to reflect possible intrusion of stratospheric ozone.

2.3. Emission data

2.3.1. Anthropogenic emissions. Anthropogenic emissions of SO_2, NO_x, CO and NMHC (non-methane hydrocarbon) for the year 2000 in Asia are derived from Streets et al. (2003) used for TRACE-P project. The emission inventory used in this study is girded at a resolution of 0.5°, and is assumed to be time-independent during simulation. Emission data are appropriately interpolated into the TCTM model grid. The total mass of NMHC is divided into individual hydrocarbons according to the specific splitting factors for East Asia (Carmichael et al., 1998). Figure 2 displays the spatial distribution of anthropogenic NO_x and VOC emissions. It can be found that most of the anthropogenic emissions are concentrated in eastern China, extending from the Yangtze Delta, through Jiangsu and Shandong Province, to the Greater Beijing district (including Beijing, Tianjing and their satellite cities). Large amounts of emissions are also released from the Pearl River Delta, northeastern China and portions of the middle reaches of the Yangtze River.

2.3.2. Biogenic emissions. Due to the limitations in observational study of biogenic emissions and the lack of vegetation leaf biomass data in China at present, in this study we adopt the biogenic emission inventory of GEIA (global emissions inventory activity, Guenther et al. (1995)), which is on a monthly basis, with $1° \times 1°$ resolution. It is appropriately segregated into the 30×30 km model grid of TCTM. This inventory includes isoprene, terpene and other unidentified compounds. Isoprene is found to be dependent on both light and leaf temperature, whereas terpene and unidentified NMHC show a strong relationship to leaf temperature. Therefore, biogenic emission displays a distinct diurnal variation, with the highest emission rate around midday and a much lower one at nighttime. To reflect these features, the emission rate is distributed to every hour over the course of a day by using the approaches of Guenther et al. (1993) in which the standard biogenic emission for isoprene is corrected by light intensity and leaf temperature, and for terpene and unidentified compounds by leaf temperature. The leaf temperature is assumed to be represented by air temperature close to the surface (air temperature at 2 m height), which is derived from MM5. Isoprene emission is assumed to be zero during the nighttime.

Figure 3 presents the horizontal distribution of total biogenic and isoprene emissions at 14:00 LT (LT = UTC + 8 h) on 14 August 2001. The large amounts of biogenic emissions are mainly concentrated in southern China (south of 33°N), portions of

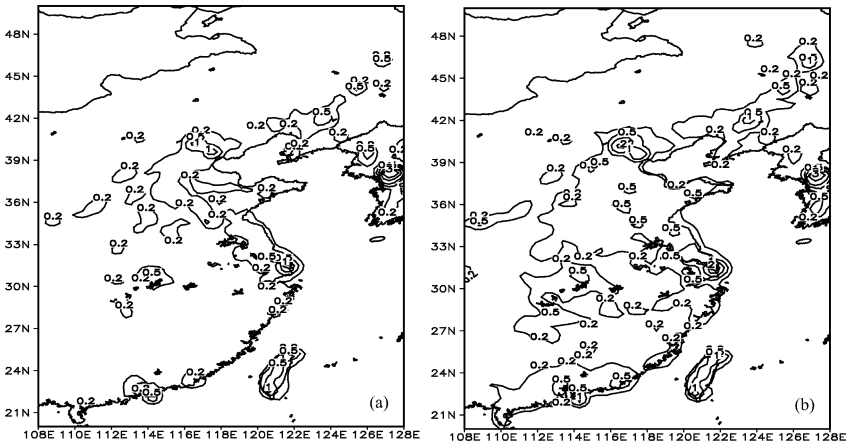

Fig 2. Anthropogenic (a) NO_x and (b) VOC emission in eastern China (unit: kg grid^{-1} s^{-1}).

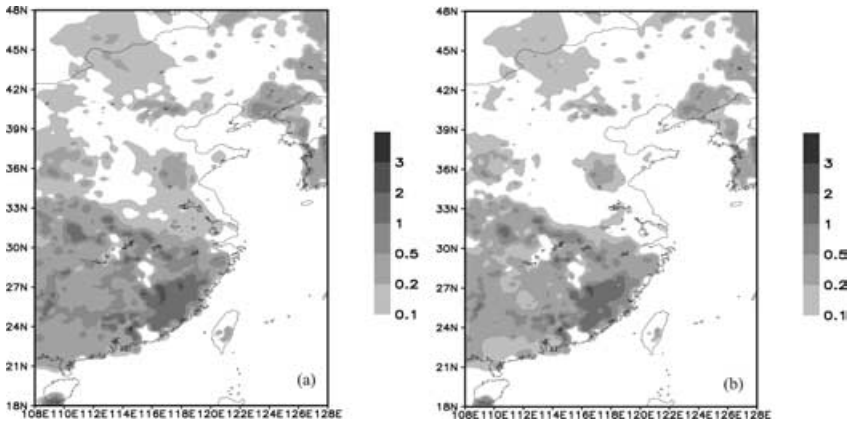

Fig 3. Biogenic emissions at 14:00 LT on 14 August 2001 (unit: kg grid^{-1} s^{-1}). (a) Total biogenic emission (isoprene + terpene + unidentified). (b) Isoprene.

northeast China, northern parts of the Greater Beijing district and the western portion of Shandong Province, in accordance with large forested areas. Compared with Fig. 2b, the proportion of biogenic to anthropogenic VOC emissions varies spatially. Biogenic emission plays a dominant role in the large rural areas of southern China, while anthropogenic VOC emission dominates the large urban and industrial areas in northern parts of China, extending consecutively from the Yangtze Delta to the Greater Beijing district. In the Pearl River Delta, the southern portion of the Yangtze Delta and northeast China, biogenic emission is nearly comparable with or even exceeds anthropogenic VOC emission. Fig. 3b shows isoprene emission in the model domain, generally consistent with the distribution pattern of total biogenic emission. Table 1 summarizes the total amount of anthropogenic and biogenic emissions within the study domain during the period of 12–16 August 2001. It clearly shows that the total biogenic VOC emission is of the same order as the anthropogenic emission, and isoprene makes up nearly 60% of the total biogenic emission. Isoprene is treated explicitly in the chemical mechanism, whereas terpene and other undefined hydrocarbons are treated according to the approach of Roselle et al. (1991). One mol of monoterpene or α-pinene is treated as 0.5 mol olefins, 6 mol paraffins and 1.5 mol higher aldehydes; 1mol undefined is treated as 0.5 mol olefins and 8.5 mol paraffins.

Although the biogenic emissions in this study cannot be completely validated due to the lack of such observations in China, they are generally representative of the major characteristics of biogenic emissions over eastern China in the summer; possible uncertainty in the emission inventory could be considered not to change the major aspects and conclusions of model estimations.

3. Model results

3.1. Synoptic features

Figure 4a shows the MM5-simulated potential height at the pressure level of 850 hPa at 14:00 LT on 14 August 2001. The isopleth of 1500 m covers most areas of eastern China, with several high-pressure systems located west of Shandong Province, northeast China and on the coastal areas of southeastern China. Such a synoptic pattern persisted for several days, and caused low wind speed, lower humidity and high temperature over a wide area of the model domain. The maximum temperature was found to exceed 33 °C in the daytime. Relatively light cloud coverage introduced sufficient radiation and favoured ozone production. There was a weak low-pressure system over a small portion of southern China, while to the north of model domain, a low-pressure system occurred and slowly moved southward as the episode progressed. The East China Sea was dominated by a cyclone, moving northwards, resulting in much precipitation over the sea. On 17 August 2001, high-pressure systems over eastern China weakened; Fig. 4b shows that the 1500 m isopleth receded eastward to the China Yellow Sea, followed by increasing wind speed and precipitation over southern China. MM5 appears to reproduce well the major features of synoptic systems, which have a large effect on ozone behaviour during this period. A detailed evaluation of the performance of MM5 will be given in Section 3.3.1.

Table 1. Total amount of anthropogenic and biogenic emissions in the study domain during the period of 12–16 August 2001 (unit: Gg)

	Anthropogenic emissions				Biogenic emissions			
Species	SO_2	NO_x	NMVOC	CO	Isoprene	Terpene	OVOC	Total
Amount	294.8	184.6	238.5	1507.3	171.6	41.6	74.4	287.6

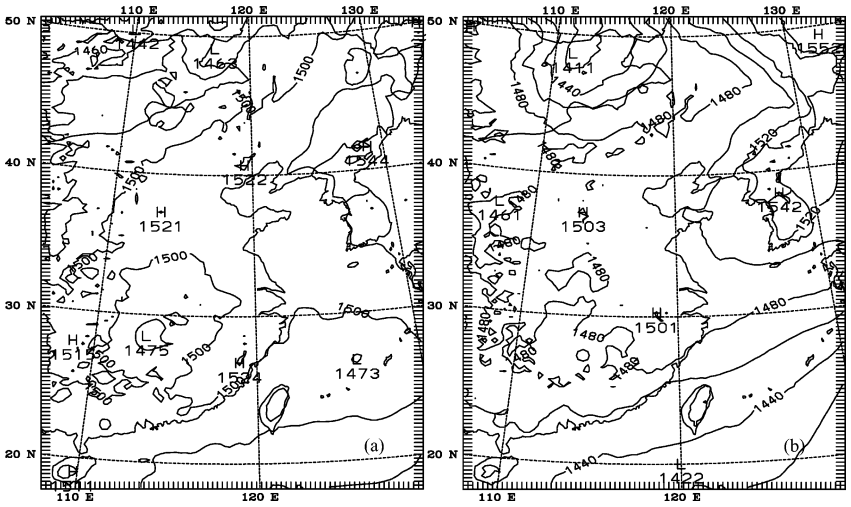

Fig 4. MM5 predicted potential height at 850 hPa level at 14:00 LT on (a) 14 August 2001 and (b) 17 August 2001.

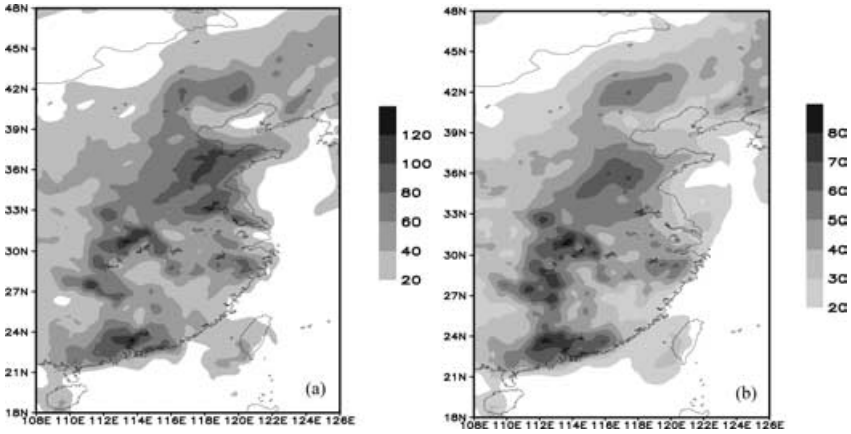

Fig 5. Predicted ozone for the first model layer: (a) at 14:00 LT on 14 August 2001 and (b) daytime ozone averaged over the 5-d period (unit: ppb).

3.2. Distribution of surface ozone over eastern China

Figure 5a presents the simulated ozone concentrations for the first model layer at 14:00 LT on 14 August 2001 when high ozone levels occurred over a wide area of eastern China, extending from the southern portion of Huabei Plain (Shandong Province), through the middle reaches of the Yangtze River (Hubei and Hunan provinces) to the Pearl River Delta, with ozone maxima reaching 126, 122 and 137 ppb respectively. Noticeably, ozone levels in Beijing and Shanghai, which contain large amounts of ozone precursors, were not so high. The lower ozone concentration in Beijing was mainly attributed to the unfavourable meteorological conditions (cloud coverage, lower temperature and higher wind speed) and ozone titration by large NO emissions. As for Shanghai, the cyclone mentioned above moved northwards with its western edge passing through Shanghai, causing relatively high wind speeds, low temperature and an easterly wind, which was characterized by a marine air mass with low ozone levels. These conditions prohibited ozone build-up in Shanghai. Further discussion will be given in the next section.

Figure 5b shows the ozone concentration of the first model layer averaged over the daytime period (10:00 LT to 17:00 LT) on 12–16 August 2001. The distribution pattern is similar to that in Fig. 5a. Large ozone concentrations were found in and in the vicinity of large cities such as Jinan, Wuhan and Guangzhou. Elevated ozone also appeared in the southern portion of the Yangtze Delta where an ozone maximum occurred on 16 August.

3.3. Comparison between simulation and observation

3.3.1. Meteorological fields. Synoptic conditions and meteorological fields play important roles in the evolution of tropospheric ozone. Therefore, an evaluation of meteorological components from the meteorological model (MM5) is necessary. Furthermore, such an evaluation will not only reveal the key features of meteorology but will also provide insightful information on ozone formation and transport for the specific episode.

Firstly, the modelled wind speed and temperature are compared with hourly observations at Jinan, Hangzhou and Gulangyu, which were conducted at the same locations as species observations (Fig. 6). The temperature at Gulangyu and wind

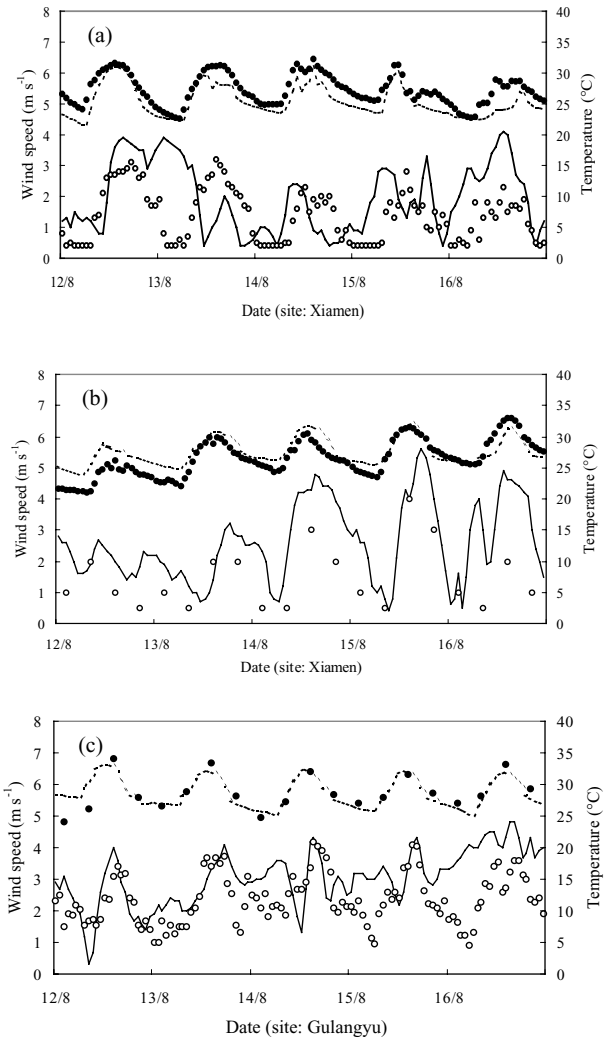

Fig 6. MM5 predicted and observed wind speed and temperature for the first model layer at (a) Jinan, (b) Hangzhou and (c) Gulangyu, during the 5-d period. Open circles and black dots represent observed wind speed and temperature, whereas solid and dashed curves represent MM5 predicted wind speed and temperature, respectively.

speed at Hangzhou were measured every 6 h each day (at 02:00, 08:00, 14:00, 20:00 LT). A general consistency can be found between simulated and observed variability of wind speed, although relatively large differences exist in detail. These discrepancies mainly result from the subscale fluctuations induced by topography, land use and urban structures, which cannot be well represented by a meteorological model with such a grid resolution. However, modelled wind speeds agree with observations quite well at the Gulangyu site, implying more influence from large-scale meteorology and a relatively homogeneous background around this site. The simulated and observed wind speeds averaged over the 5-d period (from 00:00 LT on 12 August to 23:00 LT on 16 August 2001) are 1.9 and 1.4 m s^{-1} for Jinan, 2.5 and 1.5 m s^{-1} for Hangzhou and 3.0 and 2.4 m s^{-1} for the Gulangyu site, respectively. This shows that MM5 tends to overpredict wind speed at all three sites. As for temperature, modelled averages are 25.4, 27.6 and 28.8 °C for Jinan, Hangzhou and Gulangyu, respectively, while corresponding observations are 27.2, 26.5 and 28.7 °C. Compared with wind speed, MM5 shows a better performance on temperature and has the best performance at Gulangyu for both wind speed and temperature.

To provide more information on synoptic conditions during this period, meteorological fields at four representative big cities in China (Beijing, Shanghai, Wuhan and Guangzhou) are presented in Table 2 and used for the evaluation of the performance of MM5 over a wider range of eastern China. Meteorological fields including temperature, wind direction and speed, humidity, precipitation, amount of cloud and weather description are recorded every 6 hours per day (at 02:00, 08:00, 14:00 and 20:00 LT) at the above sites. It is impossible to present all the information due to large data set, so here we chose meteorological fields at 14:00 LT on 12–16 August 2001 to demonstrate the dominant synoptic features and performance of MM5 because the meteorological conditions at this time are crucial to ozone build-up, accumulation and transport. On the other hand, as introduced in Section 3.2, Wuhan and Guangzhou experienced high ozone levels whereas Beijing and Shanghai showed lower ozone levels. Although ozone observations are not available for these regions, the synoptic conditions can provide an insight into daytime ozone production during this period.

Some conclusions can be derived from Table 2:

(1) MM5 has a good performance on temperature and relative humidity, except for Shanghai on 12 August when the temperature was overpredicted and humidity was underpredicted. Although the simulated temperature is somewhat lower than observation, there is little difference in absolute value on average. Wind speed and direction appear to be predicted quite well with the exception of Shanghai on 12 August and Wuhan on 13 August. High wind speeds at Beijing and Shanghai and lower wind speeds at Wuhan and Guangzhou are well predicted by MM5.

(2) During this period, there was no or very little precipitation over most of eastern China, both in observation and simulation. Wuhan and Guangzhou experienced low wind speed, high temperature and sufficient radiation which were favourable for ozone production. In contrast, Beijing showed high wind speeds and relatively moderate temperature that restrained ozone formation and accumulation. A similar situation occurred in Shanghai. In addition, easterlies from the East China Sea with low ozone further diminished the effectiveness of ozone production. Noticeably, the synoptic situations coincide with modelled ozone patterns (Section 3.2) quite well over most areas of eastern China.

(3) The simulated cloud fractions are generally smaller than cloud amount observed (the number in the brackets in Table 2 represents the lower cloud amount). Several factors are probably

Table 2. MM5 modelled and observed meteorological fields and weather conditions at 14:00 LT from 12 to 16 August 2001 at four big cities in China. WS is wind speed and WD wind direction. The unit of observed cloud amount is Oktas (from 0–8, see WMO code)

	WS ($m\ s^{-1}$)		WD (°)		Temp. (°C)		RH (%)		Rain ($mm\ h^{-1}$)		Cloud amount		
Date	Obs.	Calc.	Obs.	Calc.	Obs.	Calc.	Obs.	Calc.	Obs.	Calc.	Obs.	Calc.	Weather
Beijing (39.93°N, 116.27°E)													
12 Aug.	3	1.9	160	143.7	31.8	31.6	49	45.1	0	0	3 (3)	0.1	F
13 Aug.	2	0.9	140	130.6	29.6	29.8	55	54.0	0	0	2 (2)	0.1	F
14 Aug.	4	3.5	220	194.8	29.6	28.1	54	56.1	0	0	7 (0)	0.2	LC
15 Aug.	5	4.4	140	178.7	30.6	29.3	52	62.0	0	0	2 (2)	0.2	F
16 Aug.	5	4.5	220	186.3	27.8	27.6	66	69.2	0	0	8 (8)	0.3	C
Shanghai (31.4°N, 121.46°E)													
12 Aug.	3	3.2	340	214.7	25.8	29.6	81	61.2	1	0	7 (6)	0.3	C
13 Aug.	3	2.4	20	67.8	27.5	28.6	66	65.9	0	0	7 (2)	0.3	LC
14 Aug.	3	2.9	90	72.2	28.5	28.6	66	58.1	0	0	3 (2)	0.2	F
15 Aug.	3	4.2	70	115.3	29	29.1	70	63.9	0	0	6 (1)	0.3	F
16 Aug.	5	4.5	110	135.9	29.9	29.4	81	66.4	2	1	6 (3)	0.3	F
Wuhan (30.93°N, 114.12°E)													
12 Aug.	1	1.7	20	28.1	29	28.9	45	56.9	0	0	7 (2)	0.3	LC
13 Aug.	1	0.8	290	119.7	31.9	29.4	42	55.5	0	0	3 (3)	0.1	F
14 Aug.	2	2.3	160	115.5	31	30.6	56	54.2	0	0	7 (0)	0.1	LC
15 Aug.	2	1.2	90	70	30.7	29.9	62	56.1	0	0	6 (6)	0.1	F
16 Aug.	1	0.5	140	90	31.5	32.6	57	54.7	0	0	6 (6)	0.1	F
Guangzhou (23.13°N, 113.31°E)													
12 Aug.	3	2.8	90	178	32.7	32.4	58	55	0	0	7 (7)	0.2	C
13 Aug.	1	0.5	270	243	33	31.1	56	54.3	0	0	6 (5)	0.2	F
14 Aug.	0	0.6	0	270	33.4	31	55	60.3	0	0	6 (6)	0.3	F
15 Aug.	2	0.3	340	225	33	30.5	61	49	0	0	7 (6)	0.5	C
16 Aug.	1	1.5	360	0	32.1	30.9	59	52.2	0	0	7 (5)	0.5	C

responsible for these discrepancies. Firstly, cloudiness may be less well reproduced by the model due to the inherent limitation of current meteorological models in the prediction of cloud processes, especially for subscale cumulus convection. Secondly, the definitions of these two variables are somewhat different; the modelled cloud fraction represents cloud percentage within a specific model grid, whereas the amount of cloud represents cloud percentage within the range of vision which may exceed a certain grid area. Thirdly, the observed amount of cloud is of limited accuracy owing to manual observation. Therefore, the observed weather report is used as an additional indicator in the evaluation of modelled cloudiness. In Table 2, C, LC and F represent cloudy, little cloud and fine weather respectively. It can be found that simulated cloudiness is in a better agreement with the weather report than with total cloud amount. Figure 7 shows the predicted cloud fraction and observed weather condition and total cloud amount at 14:00 LT on 14 August 2001. It indicates that the dominant weather conditions during this period are reasonably well predicted by the model.

3.3.2. Ozone and related trace gases (NO_2 and SO_2). Before model evaluation, it should be pointed out that ozone measurements are still limited in China because ozone is not an item requiring regular monitoring by SEPAC (the State Environmental Protection Administration of China) at present. Ozone measurements in rural or remote areas are even scarcer. Currently, ozone measurements are generally supported by local governments and are often conducted in or in the vicinity of urban areas. In this study, three monitoring sites located in suburban areas of Jinan, Hangzhou and Xiamen are available and used for model comparison.

Jinan (117°02′E, 36°42′N), the capital of Shandong Province, is located in the southern Huabei Plain, with the Yellow River passing by its northern edge and mountains to the south. The monitoring site is on the top of a five-floor building, about 20 m above ground. This site is about 3 km away from the urban centre. Hangzhou (120°12′E, 30°18′N) is the capital of Zhejiang Province, 210 km southwest of Shanghai. The monitoring site is located in a suburban area which is about 4 km away from the urban centre; the sampling height is about 10 m. Gulangyu (118°06′E, 24°27′N) is a small scenic island with a population of 20 000, which is about 6 km southwest of the urban centre of Xiamen (a coastal city along the South China Sea). There are no automobiles or industry on Gulangyu Island; bicycles and electric cars provide the main transportation. The instruments are placed on a small hill with a height of 40 m. This site reflects a relatively clean background, influenced by both marine and continental air masses.

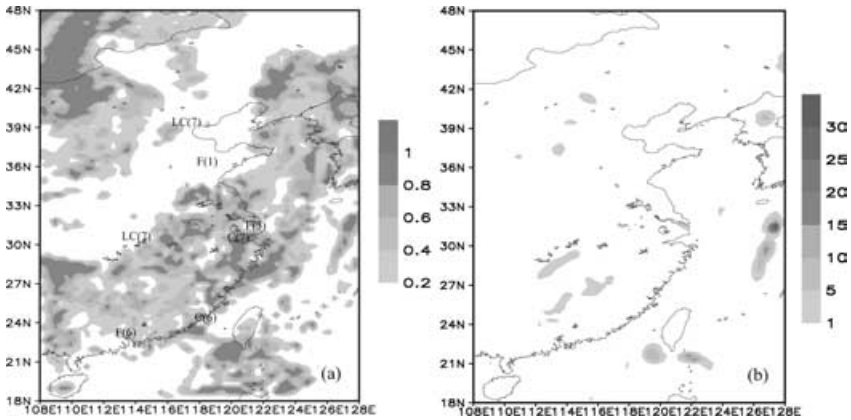

Fig 7. (a) Model predicted cloud fraction and observed weather conditions and amount of cloud. (b) Predicted precipitation (unit: mm h^{-1}). The time is 14:00LT on 14 August 2001. Symbols C, LC and F in (a) represent cloudy, little cloud and fine weather in the observations. The number in the bracket is the observed total cloud amount.

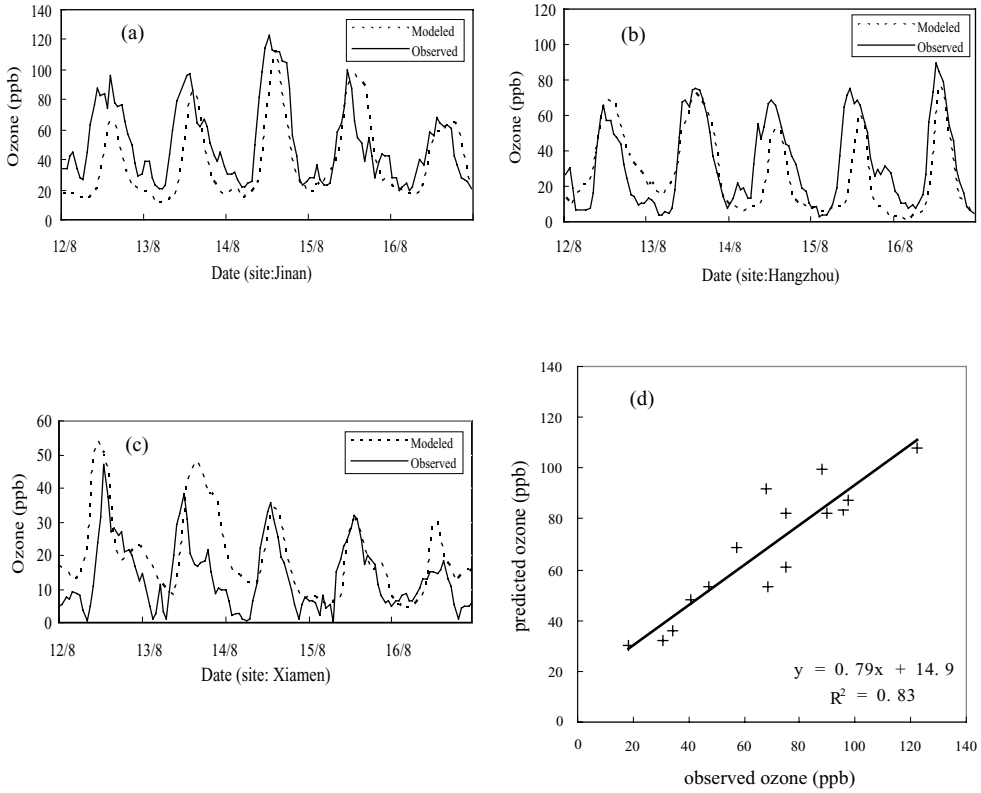

Fig 8. Model predicted and observed hourly O_3 concentrations at (a) Jinan, (b) Hangzhou, (c) Gulangyu and (d) a scatter plot of observed and predicted daily maximum ozone at three sites, during the 5-d period.

Ozone concentration was measured by a UV photometry analyser (model 49C of the Thermo Electron Corporation) at three monitoring sites, following the standard procedure of measurement implemented by SEPAC.

Figures 8a–c show the predicted and observed hourly ozone concentrations at the three monitoring sites. The correlation coefficients for Jinan, Hangzhou and Gulangyu sites are 0.69, 0.75 and 0.60, respectively. Although a significant correlation between simulation and observation is obtained, systematic discrepancies still exist. Table 3 presents the observed and modelled ozone concentrations averaged over the 5 d (from 00:00 LT on 12 August to 23:00 LT on 16 August 2001) and over the daytime period (10:00 LT to 17:00 LT) for the 5 d.

Table 3 shows that for the 5-d averages, the model tends to underpredict the observed ozone by 24% and 20% at Jinan and Hangzhou sites, respectively, and overpredict by 25% at Gulangyu site. For the daytime averages, model performance is better, with discrepancies within 20% at all sites.

Underprediction for high ozone observation and overprediction for low ones are common features of 3-D regional models

Table 3. Simulated and observed average ozone concentrations (unit: ppb) at three sites

	5-d averaged			Daytime averaged		
Site	Model	Obs.	Model/obs.	Model	Obs.	Model/obs.
Jinan	39.2	51.6	0.76	67.2	79.7	0.84
Hangzhou	26.2	32.7	0.80	51.5	64.0	0.81
Gulangyu	18.5	13.8	1.34	28.5	24.2	1.18
Ave. over sites	28.0	32.7	0.86	49.1	55.9	0.88

(Brasseur et al., 1999). Underprediction often occurs near urban sources, which is mainly attributed to the limitation of a regional model in reproducing subscale urban plumes and incommensurability in the comparison of point measurements with volume averages by the model (Schere and Wayland, 1989; McKeen et al., 1991; Roselle and Schere, 1995). Overprediction is found mostly at remote locations, which is probably related to the low model resolution and inherent overprediction of OH concentration by regional scale models at lower NO_x levels (Sillman et al., 1990; McKeen et al., 1997). Nevertheless, other uncertainties in this model simulation, such as boundary layer evolution and cloudiness, magnitude and diurnal cycle of emission, as well as inherent numerical diffusion related to the advection scheme, may also contribute to the above discrepancies in ozone concentration.

Although some differences exist in absolute values, Figs 8a–c show a general agreement between the observed and predicted ozone tendency, indicating the model's capacity to capture major processes dominating ozone behaviour and to reproduce day-to-day ozone variability associated with the evolution of synoptic conditions. Ozone maxima are well reproduced by the model at Jinan on 14 August, at Hangzhou on 16 August and at Gulangyu on 12 August 2001, well consistent with the favourable synoptic situations on those days. This also implies that ozone behaviour is strongly influenced by the evolution of synoptic conditions during this period.

Figure 8d shows a scatter plot of the predicted and observed daily ozone maximum for all three monitoring sites during the 5-d period. It indicates that the model is able to capture the general features of diurnal ozone variations and there is no significant bias between model prediction and observation.

Figure 9 shows the time-series of observed and predicted hourly NO_2 and SO_2 concentrations at Jinan and Hangzhou sites, which were measured with ozone simultaneously at the same locations. NO_2 and SO_2 were measured respectively by a chemiluminescence NO–NO_2–NO_x analyser (model 42C) and a pulsed fluorescence SO_2 analyser (model 43C) of the Thermo Electron Corporation. A general agreement can be found between the observed and simulated NO_2 trend. Diurnal variation of NO_2 resulting from the cycle of boundary layer and chemistry is well reflected in both observation and model simulation. It is not surprising to see the larger differences in the early morning and late afternoon because the NO_x emissions from transportation are abruptly elevated around rush hour, whereas in the model, NO_x emission is treated constant and grid averaged, causing less variability in NO_2 concentration. SO_2 concentration is

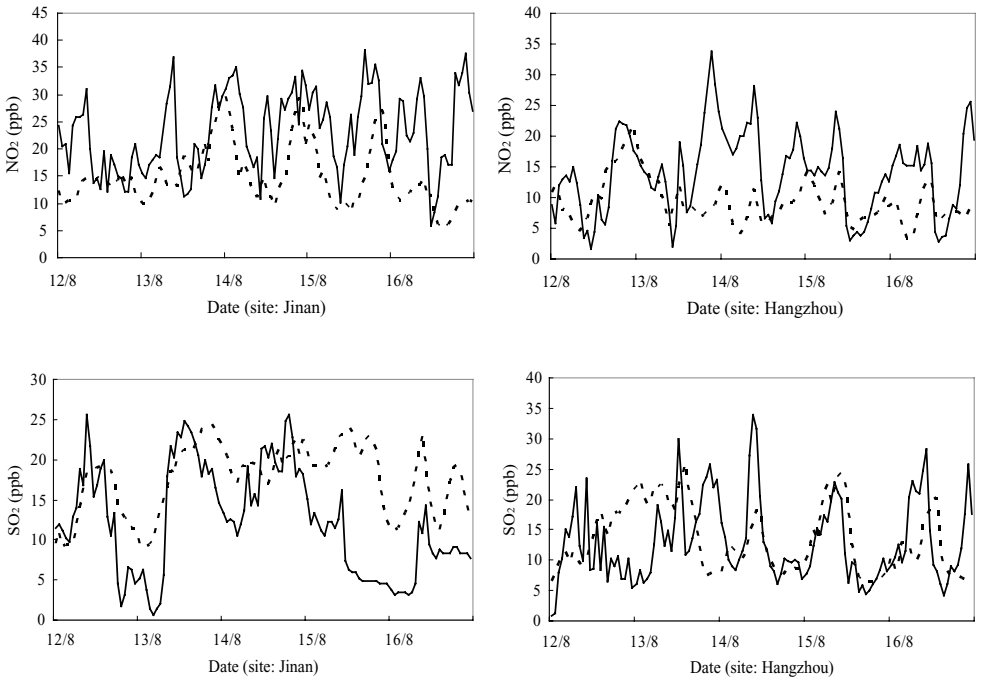

Fig 9. Model predicted (dashed) and observed (solid) hourly NO_2 and SO_2concentrations at Jinan and Hangzhou during the 5-d period.

Table 4. Simulated and observed average NO_2 and SO_2 concentrations (unit: ppb) at two sites

	NO_2						SO_2					
	5-d averaged			Daytime averaged			5-d averaged			Daytime averaged		
Site	Mod.	Obs.	Mod./obs.	Mod.	Obs.	Mod./obs.	Mod.	Obs.	Mod./obs.	Mod.	Obs.	Mod./obs.
Jinan	14.9	22.9	0.65	12.6	18.9	0.67	17.5	12.2	1.43	19.1	14.9	1.28
Hangzhou	9.4	14	0.67	8.5	8.6	0.99	13.5	13.0	1.03	15.0	12.4	1.21
Ave. over sites	12.2	18.5	0.66	10.6	13.8	0.77	15.5	12.6	1.23	17.1	13.7	1.24

reproduced by the model fairly well in terms of day-to-day and diurnal variability with the exception of 15 August at Jinan site and 12 August at Hangzhou. Table 4 presents the observed and modelled averages over the 5 d and the daytime period for the 5 d for NO_2 and SO_2 at Jinan and Hangzhou, corresponding to Table 3. It shows that the model tends to generally underpredict NO_2 observation up to 35% at the two sites, but model results for NO_2 in the daytime appear to be better than that for the whole day. SO_2 concentration averaged over 5 d is overpredicted by 30% at Jinan, and quite well simulated at Hangzhou. The above discrepancies in primary pollutants are attributed to the effect of subscale urban plume and uncertainties in the emission database and predicted boundary layer variables.

Despite some discrepancies in model validation, they appear to be reasonably within the expected uncertainty limits and of an acceptable scope. Given a horizontal grid size of 30 km in a regional model, the results appear to be satisfactory. In general, meteorological fields modelled by MM5 are reasonably good. TCTM is able to represent most of the major features involved in ozone evolution and reasonably reproduce day-to-day and diurnal variations of ozone and other related trace species. Given such a validation result, we have more confidence in the reliability of this model's performance and subsequent model studies.

4. Impact of biogenic emissions on ozone concentration

To investigate the impact of biogenic emission on regional ozone, in addition to the base case mentioned above (with both anthropogenic and biogenic emissions), two sensitivity model simulations were performed with different emission data sets. The first one (case 1) included only anthropogenic NO_x and VOC emissions; the second one (case 2) included anthropogenic NO_x and biogenic emissions with anthropogenic VOC emission eliminated. The base case was used for reference. The meteorological data and other model parameters were identical for the above three simulations.

4.1. Sensitivity of ozone concentration to biogenic emission

Figure 10a illustrates the differences (base case minus case 1) in daytime (10:00–17:00 LT) averaged ozone concentrations for the lowest model layer from 12 to 16 August 2001. Remarkable increases of ozone are predicted over wide areas of eastern China when biogenic emissions are taken into account. Large increases are found to occur in the middle reaches of the Yangtze River, the Pearl River Delta, the southern portion of the Yangtze Delta and northeastern parts of China. The ozone increment in all the above areas exceeds 20 ppb, with a maximum up to 30 ppb appearing to the northwest of Wuhan (capital of Hubei Province, in the middle reaches of the Yangtze River) and in portions of northeast China. These areas are characterized by high coverage of forest, influence by human activities, as well as favourable meteorological conditions. It is noticeable that ozone shows little change over large rural areas of southern China even though large amounts of biogenic emissions exist there, implying less VOC sensitivity in those areas.

A small ozone response to biogenic emissions also occurs in the northern Huabei Plain (including Beijing and Tianjing), Shanghai and small portions of southern China, due to the relatively small amount of biogenic emission or unfavourable meteorological conditions discussed above. Over very clean vegetated areas, ozone shows a little decrease, as a result of its interaction with vegetative hydrocarbons.

The peroxyacetyl nitrate (PAN) concentration shows an evident increase as well (not illustrated), with average increase of 1.5 ppb for the daytime period of 5 d, and the areas of PAN increase closely correspond to those of ozone. A significant increase in PAN implies the potential influence of biogenic sources on atmospheric composition on a larger scale through the transport of precursor storage.

The enhancement of ozone is mainly attributed to the evident increase in the HO_x radicals ($OH + HO_2 + RO_2$, RO_2 being the peroxyalkyl radical) by biogenic emission, which leads to higher activity of the photochemical system. Figure 10b presents the per cent increase from case 1 (defined as $(C_{base} - C_{case1})/C_{case1}$) in daytime HO_x concentration averaged over the 5-d period. HO_x is increased by a factor of 1 to 8 in most vegetated areas. The largest increase up to a factor of 8 appears in portions of northeast China, the middle reaches of the Yangtze River and the southern portion of the Yangtze Delta, in accordance with the regions seeing largest ozone enhancement.

Elevated ozone in biogenic source regions can be transported over a long distance, leading to an increase of ozone levels

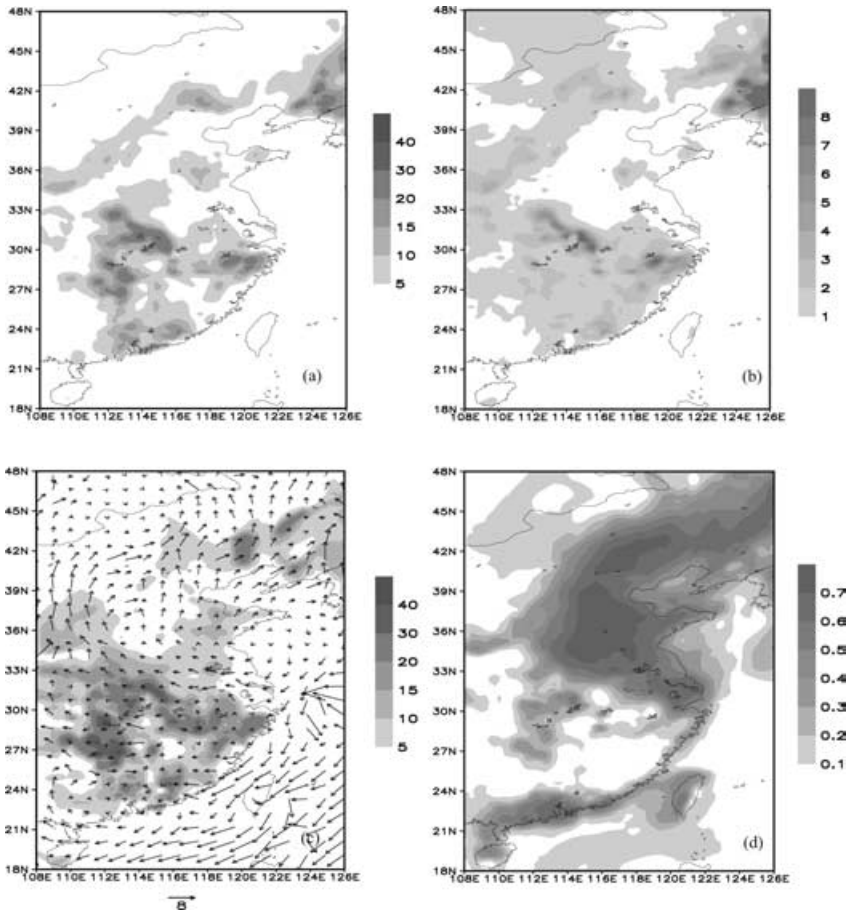

Fig 10. Model predictions for: (a) differences in daytime averaged ozone concentration over the 5-d period between the base case and case 1 (base case minus case 1, unit: ppb), (b) per cent increase in daytime averaged HO_x radical from case 1, (c) wind vector and difference in ozone concentration between the base case and case 1, at 12:00 LT on 14 August 2001, (d) per cent decrease in daytime averaged ozone concentration between the base case and case 2. Values are for the first model layer.

downwind. Figure 10a shows that in some portions of mid-China (33°N–36°N, 112°E–116°E) where biogenic emissions are scarce (shown in Fig. 3), daytime average ozone enhancement reaches as much as 5–10 ppb due to the transport of elevated ozone from southeastern regions where large ozone increases due to biogenic emission are found. Figure 10c shows the ozone increase and wind vector at 12:00 LT on 14 August 2001; ozone transport from biogenic source regions to downwind areas can be found.

Figure 10d shows the per cent decrease from the base case (defined as $(C_{base} - C_{case2})/C_{base}$) in daytime average ozone concentration when only anthropogenic NO_x and biogenic emissions are taken into account. In most rural areas of southern China, ozone levels experience little change with per cent decrease $<10\%$. An apparent decrease of 40–70% is found in most urban and industrial regions of northern China, the Pearl River Delta, the middle reaches of the Yangtze River and the Yangtze Delta. However, in wide transitional regions between urban and rural areas, the per cent ozone reduction is only 10–30%, implying that biogenic emission may build up considerable ozone levels itself in polluted areas.

Among the three categories of biogenic emission, isoprene is found to be the most important species contributing to ozone formation due to its large percentage of total biogenic emissions and high chemical reactivity.

4.2. Relationship between ozone and precursors

Ozone formation is well known to be nonlinear and controlled by precursors, i.e. NO_x and VOC (Liu et al., 1987). Such a relationship was revealed in previous studies (Sillman et al., 1990; Sillman, 1995), that is, ozone increases with increasing NO_x and is nearly insensitive to hydrocarbons for low-NO_x regimes (NO_x limited), whereas ozone decreases with increasing NO_x and increases with increasing hydrocarbon for high-NO_x regimes (VOC limited). There exists a 'turnover' value or span in NO_x concentration, which separates low-NO_x and high-NO_x regimes and exhibits a peak of ozone formation (Roselle and Schere, 1995). The 'turnover' depends on a series of factors including emissions, chemical activity, as well as meteorological conditions, and varies spatially and temporally (Vogel et al., 1999).

Figure 11 presents a scatter plot of O_3 versus NO_x and NO_y concentrations for the first model layer at 14:00 LT on 14 August, for the base case and case 1. In total, 2488 grid points are selected, eliminating grid points with ozone value below 40 ppb which are less representative of typical photochemistry.

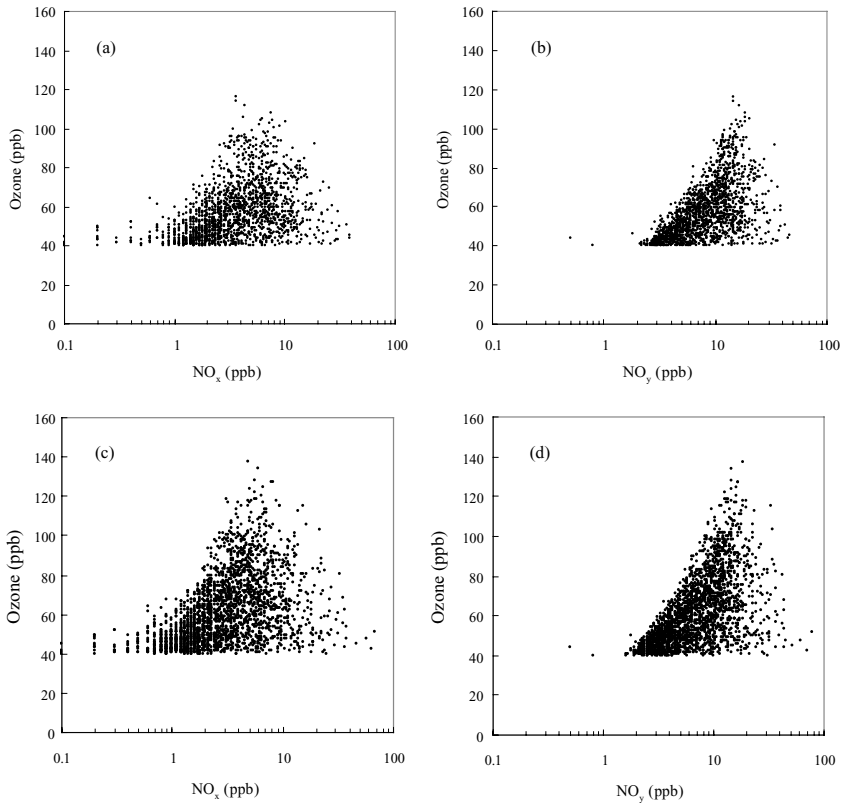

Fig 11. Scatter plot of predicted ozone versus NO_x and NO_y concentrations at 14:00 LT on 14 August 2001: (a) and (b) for case 1, (c) and (d) for the base case.

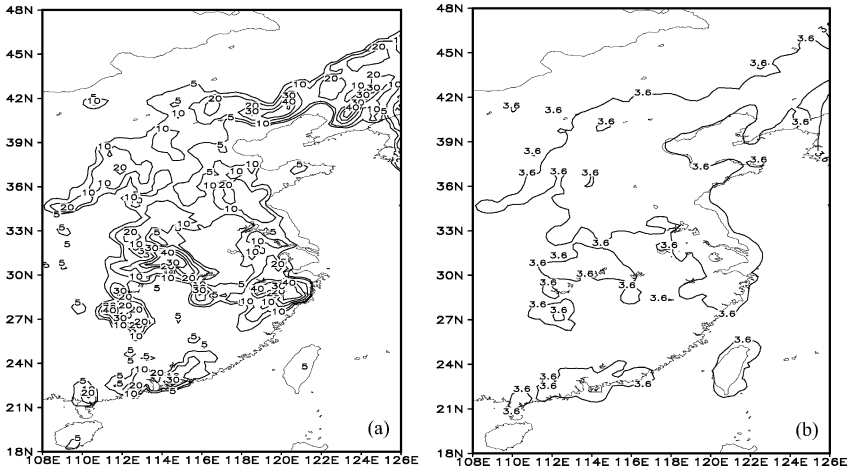

Fig 12. Model predictions for: (a) differences in ozone concentration (base case minus case 1) and (b) NO_x concentration in case 1. At 14:00 LT on 14 August 2001, for the first model layer (unit: ppb).

For the base case (Figs 11c and d), a relationship can be distinguished clearly, i.e. ozone increases as NO_x increases up to 4.9 ppb and then decreases as NO_x goes on increasing. For NO_y, a 'turnover' value is around 18.7 ppb. This relationship is similar to the results of previous studies in which the 'turnover' values around 5 ppb for NO_x and 20 ppb for NO_y were found over the United States during the summer (McKeen et al., 1991; Sillman et al., 1990; Roselle and Schere, 1995). Noticeably, 'turnover' values are apparently enhanced by biogenic emissions, from 3.6 ppb and 14.4 ppb (case 1) to 4.9 ppb and 18.7 ppb (base case) for NO_x and NO_y, respectively. The ozone maximum rises from 116 ppb for case 1 to 137 ppb for the base case as well.

Figure 12 shows a corresponding picture of NO_x concentration for case 1 and the difference in ozone concentration (base case minus case 1) at 14:00 LT on 14 August 2001. Interestingly, ozone increase is mainly confined to the areas where NO_x concentration is around or more than 3.6 ppb, related to high NO_x emission (in or in the vicinity of big cities and industrial bases), whereas less ozone response is found in broad rural areas of southern China with relatively low NO_x levels (<3.6 ppb).

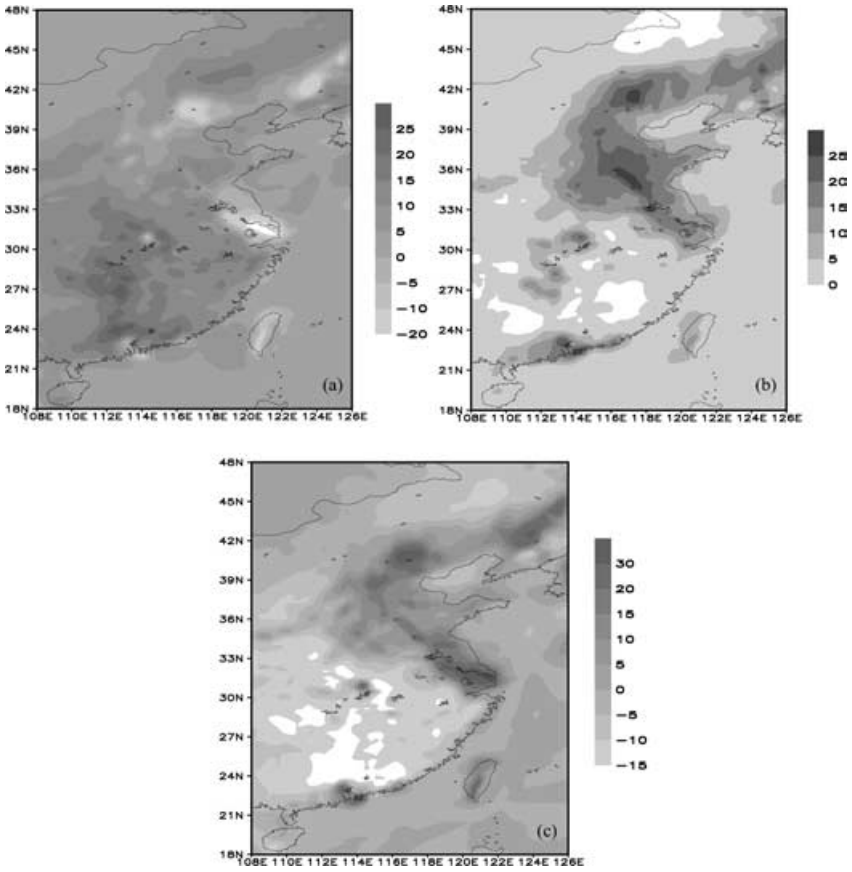

Fig 13. Predicted (a) ozone decrease from base case with 50% reduction in NO_x emission, (b) ozone decrease from base case with 50% reduction in VOC emission, (c) ozone decrease from 50% reduction in VOC emission minus that from 50% reduction in NO_x emission. The base case includes both anthropogenic (NO_x, VOC) and biogenic emissions.

This aspect is well consistent with the relationship discussed in Fig. 11. Ozone in some areas does not follow this rule, probably due to the influence of transport processes, small biogenic emissions and inactive photochemistry associated with unfavourable meteorological conditions.

5. Sensitivity of ozone to reduction in anthropogenic NO_x and VOC emissions

Whether ozone is sensitive to the reduction of NO_x or VOC emissions is an important issue for emission abatement strategies. However, ozone abatement becomes a complicated intertwining of meteorology, chemistry and biology (Brasseur et al., 1999). Figure 12 gives a preliminary image of VOC-sensitive areas over eastern China. In this section, more model simulations are conducted to further identify the NO_x-limited and VOC-limited regimes over eastern China, and to investigate how and to what extent biogenic emission affects the response of ozone to emission reduction scenarios.

To attain this goal, a series of simulations are carried out with operational emission schemes: 50% reduction in each anthropogenic NO_x or VOC emission, respectively, both with and without biogenic emissions. Results are presented in terms of daytime (10:00–17:00 LT) averaged ozone concentrations of the first model layer for the 5-d period of 12–16 August 2001. The meteorological, initial and boundary conditions are identical for these simulations.

The sensitivity simulations with biogenic emissions are shown in Fig. 13. Figures 13a and b show the ozone decrease from the base case (Fig. 5b) with 50% reduction in either anthropogenic NO_x or VOC emissions. Figure 13a clearly shows that with 50% reduction in NO_x emission, ozone is decreased by 10–25 ppb over most of model domains except for a few regions which are characterized by urban or industry with large NO_x emissions, such as the Yangtze Delta, portions of the Pearl River Delta, the Greater Beijing district, portions of northeast China and the middle reaches of the Yangtze River. On the contrary, these areas experience an ozone increase of 5–20 ppb.

Figure 13b shows that a 50% reduction in VOC emission leads to evident ozone decrease of 10–25 ppb over large northern parts of eastern China, portions of the middle reaches of the Yangtze River, the Yangtze Delta and the Pearl River Delta. A large ozone decrease exceeding 15 ppb is found within or in the vicinity of urban and industrial areas mentioned above. Most of the rural areas in southern China where large biogenic emission exists show little or no change in ozone concentration.

Figure 13c illustrates the differences in ozone decrease due to 50% reduction of VOC emission minus that due to 50% reduction

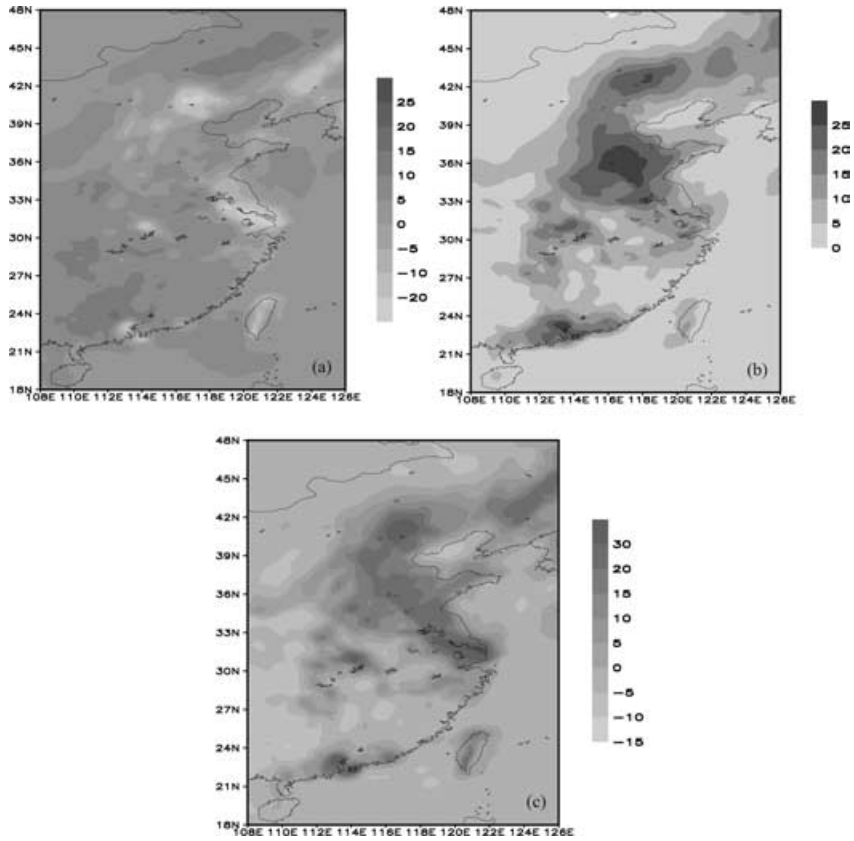

Fig 14. Predicted (a) ozone decrease from case 1 with 50% reduction in NO_x emission, (b) ozone decrease from case 1 with 50% reduction in VOC emission, (c) ozone decrease from 50% reduction in VOC emission minus that from 50% reduction in NO_x emission, without taking biogenic emission into account. Case 1 includes only anthropogenic NO_x and VOC emissions.

of NO_x emission, showing a clear image of NO_x- and VOC-limited regimes over eastern China in the presence of biogenic emissions.

It is found that ozone experiences more decrease from a 50% reduction of NO_x emission than that from a 50% reduction of VOC emission in most of the rural areas of middle and southern China and portions of northeast China, indicating that NO_x limitation generally applies in those regions. Large northern parts of eastern China (north of 30°N) where clusters of cities mixed with industrial bases are located are clearly VOC limited, generally consistent with the spatial distribution of anthropogenic emissions (Fig. 2a).

There exist some transitional regions between cities and rural areas where ozone response is nearly equivalent to reductions in both NO_x and VOC emission, including the areas lying between 30°N and 35°N in mid-China, portions of northeastern China and the Pearl River Delta, as well as the western portion of the Yangtze Delta. Figure 13 also shows that VOC-limited regimes can be comparable with NO_x-limited ones over eastern China, implying the influence of increasing NO_x emissions and the decrease of rural areas in northern China in recent years.

Figure 14 presents the corresponding simulations without considering biogenic emissions. Figure 14a shows that although the pattern is similar to that of Fig. 13a, the magnitude and extent of ozone decrease becomes smaller, from a maximum of 25 ppb in Fig. 13a to 10 ppb in Fig. 14a over most of the rural areas. Comparison of Figs 13b and 14b shows VOC-limited areas are apparently reduced in Fig. 13a. Figure 14c presents the differences of ozone decrease from 50% reduction of VOC emission minus that from 50% reduction of NO_x emission, showing the image of NO_x- and VOC-limited regimes over eastern China with only anthropogenic emissions taken into account. NO_x-limited regimes are mostly confined to rural areas of southern China, whereas VOC limitation applies over broad areas of northern parts of China. Very VOC-limited regimes are the northern portion of the Yangtze Delta, the Pearl River Delta, a portion of the middle reaches of the Yangtze River and the Greater Beijing district where large cities are located. Figure 14c may also provide an implication of sensitivity of ozone to emission changes at times when biogenic emission is not so active (late autumn, winter, early spring).

From the comparison of Figs 13c and 14c we find that NO_x-limited areas are apparently enlarged when biogenic emission is taken into account (Fig. 13c), with the northern edge extending far northward, reaching 32°N in general, and former NO_x-limited areas in southern China becoming more NO_x dependent, with ozone decrease varying from 5–10 ppb to 5–20 ppb. Apparent changes occur in the middle reaches of the Yangtze River (in the vicinity of Wuhan), the southern portion of the Yangtze Delta and portions of northeast China where a former VOC-limited

regime completely changes its attribution to NO_x limitation, due to the large biogenic emission released from forest in those areas. On the contrary, VOC-limited areas are apparently decreased, receding northward. Even in those urban areas, the VOC-limited condition is somewhat mitigated and some of the suburban areas become transitional or NO_x limited. These results are consistent with that of Pierce et al. (1998) in which a tendency to shift from VOC to NO_x limitation appears due to biogenic emission over eastern America in summer.

This study reveals the fact that there exist quite different emission reduction scenarios with and without including biogenic emission over eastern China, suggesting a potential larger impact of NO_x emission in the presence of biogenic emissions. Considering the current expansion of the economy and number of motor vehicles in China, NO_x and VOC emissions will both increase in the future, which may enhance the levels of ozone and related oxidants both in rural areas of southern China and most parts of northern China. This trend will consequently aggravate photochemical pollution in China which will have adverse effects on the ecosystem and agriculture, as well on air quality. Therefore, emission control strategies must be reasonably and effectively designed by taking into account not only anthropogenic but also biogenic emissions.

Although this work focuses on a particular episode, it is conceivable that the impact of biogenic emissions will be felt whenever favourable meteorological conditions occur during the growing season (spring, summer and early autumn). Therefore, biogenic emissions are expected to have a long-term influence on regional chemical systems and emission control strategies.

6. Conclusions and discussions

A tropospheric chemistry and transport model (TCTM) driven by MM5 was utilized to investigate ozone behaviour and the impact of biogenic emission over eastern China during a typical episode in August 2001. Elevated ozone was found over large areas of eastern China, extending from the southern Huabei Plain, through the middle reaches of the Yangtze River, the southern portion of the Yangtze Delta to the Pearl River Delta, coinciding with major economically developing regions. Model predictions show a generally good agreement with observations both in meteorological fields and ozone concentration, indicating a good capacity of this model system to reproduce major processes of ozone evolution.

The role of biogenic emission in photochemistry has been investigated through sensitivity model simulations, showing a significant contribution to ozone increase in the daytime. The ozone response to biogenic emission varies spatially, with more sensitivity in high-NO_x areas and less sensitivity in relatively low-NO_x areas. Biogenic emission may enhance ozone levels downwind through transport processes, suggesting its potential influence on a larger spatial scale.

Sensitivity of ozone to the reduction of NO_x and VOC emissions has been identified through a series of model simulations. Generally, NO_x limitation applies over broad rural areas of southern China, portions of middle China and northeast China, whereas VOC limitation applies over most of northern China. Extreme VOC-limited regimes coincide closely with intense human activities, such as the Greater Beijing district, the northern portion of the Yangtze Delta and the Pearl River Delta.

A general tendency towards more NO_x limitation and less VOC limitation is found when taking biogenic emissions into account. The region with NO_x-limited conditions is apparently enlarged and intensified by biogenic emission over most of eastern China. Some regions completely shift to NO_x limitation from VOC limitation, such as the southern portion of the Yangtze Delta, portions of the middle reaches of the Yangtze River and northeast China. This study indicates the potential importance and influence of biogenic emission on photochemistry, ozone and oxidants, as well as emission control strategies over eastern China in the growing season.

7. Acknowledgments

The authors acknowledge Eryi Wang, Xiaozhe Tan, Xiaoxiong Wang and Wanli Ma for providing observational data in China. We would also like to thank Dr Jung-hun Woo for supplying emission database for this study.

References

Akimoto, H., Mukai, H., Nishikawa, M., Murano, K., Hatakeyama, S. et al. 1996. Long-range transport of ozone in the East Asian Pacific rim region. *J. Geophys. Res.* **101**, 1999–2010.

Brasseur, G. P., Orlando, J. J. and Tyndall, G. S. 1999. In: *Atmospheric Chemistry and Global Change*. Oxford University Press, Oxford, 483–484.

Carmichael, G. R., Uno, I., Phadnis, M. J., Zhang, Y. and Young, S. W. 1998. Tropospheric ozone production and transport in spring time in east Asia. *J. Geophys. Res.* **103**, 10649–10671.

Carter, W. P. L. 1996. Condensed atmospheric photooxidation mechanism for isoprene. *Atmos. Environ.* **30**, 4275–4290.

Chameides, W. L., Li, X. S., Tang, X. Y., Zhou, X. J., Luo, C. et al. 1999. Is ozone pollution affecting crop fields in China? *Geophys. Res. Lett.* **26**, 867–870.

Chameides, W. L., Lindsay, R. W., Richardson, J. and Kiang, C. S. 1988. The role of biogenic hydrocarbons in urban photochemical smog: Atlanta as a case study. *Science* **241**, 1473–1475.

Chang, J. S., Brost, R. A., Isaksen, I. S. A., Madronich, S., Middleton, P. et al. 1987. A three dimensional Eulerian acid deposition model: physical concepts and formulation. *J. Geophys. Res.* **92**, 14 681–14 700.

Dodge, M. C. 1977. *Effect of Selected Parameters on Predictions of a Photochemical Model*. Report EPA-600/3–77-048, US Environmental. Protection Agency, Research Triangle Park, NC.

Elliott, S., Blake, D. R., Duce, R. A., Lai, C. A., McCreary, I. et al. 1997. Motorization of China implies changes in Pacific air chemistry and primary production. *Geophys. Res. Lett.* **24**, 2671–2674.

Gery, M. W., Whitten, G. Z., Killus, J. P. and Dodge, M. C. 1989. A photochemical kinetics mechanism for urban and regional scale computer modeling. *J. Geophys. Res.* **94**, 12 925–12 956.

Gipson, G. L. and Young, J. O. 1999. *Gas-phase Chemistry of the EPA Models-3 Community Multiscale Air Quality*. (CMAQ) Modeling System, EPA/600/R-99/030 Environmental Protection Agency, Atmospheric Modelling Division, Research Triangle Park, NC.

Grell, G. A., Dudhia, J. and Stauffer, D. R. 1994. *A Description of the Fifth-generation Penn State/NCAR Mesoscale Model (MM5)*. NCAR Technical Note NCAR/TN-398+STR National Center for Atmospheric Research, Boulder, CO.

Guenther, A., Hewitt, C., Erickson, D., Fall, R., Geron, C. et al. 1995. A global model of natural volatile organic compound emissions. *J. Geophys. Res.* **100**, 8873–8892.

Guenther, A., Zimmerman, P., Harley, P., Monson, R. and Fall, R. 1993. Isoprene and monoterpene emission rate variability: model evaluation and sensitivity analysis. *J. Geophys. Res.* **98**, 12 609–12 617.

Han, Z. W., Hu, F., Zhang, M. G. and Zhu, J. 2002. Model study of the effect of soil NO emissions on surface ozone. *Acta Meteorol. Sinica* **164**, 470–480.

Jacob, D. J., Logan, J. A. and Murti, P. P. 1999. Effect of rising Asian emissions on surface ozone in the United States. *Geophys. Res. Lett.* **26**, 2175–2178.

Lei, X. E. and Chang, J. S. 1992a. A high resolution model for chemical species exchange in troposphere. *Acta Meteorol. Sinica* **6**, 479–490.

Lei, X. E. and Chang, J. S. 1992b. A numerical study on dry deposition processes with canopy layer. *Adv. Atmos. Sci.* **9**, 460–469.

Lelieveld, J. and Dentener, F. J. 2000. What controls tropospheric ozone? *J. Geophys. Res.* **105**, 3531–3551.

Levy, H., 1971. Normal atmosphere: large radical and formaldehyde concentrations predicted. *Science* **173**, 141–143.

Liu, S. C., McKeen, S. A., Hsie, E. Y., Lin, X., Kelly, K. K. et al. 1996. Model study of tropospheric trace species distributions during PEM-West A. *J. Geophys. Res.* **101**, 2073–2085.

Liu, S. C., Trainer, M., Fehsenfeld, F. C., Parrish, D. D., Williams, E. J. et al. 1987. Ozone production in the rural troposphere and implications for regional and global ozone distributions. *J. Geophys. Res.* **92**, 4191–4207.

Logan, J. A. 1989. Ozone in rural areas of the United States. *J. Geophys. Res.* **94**, 8511–8532.

Luo, C., St John, J. C., Zhou, X. J., Lam, K. S., Wang, T. et al. 2000. A nonurban ozone air pollution episode over eastern China: observations and model simulations. *J. Geophys. Res.* **105**, 1889–1908.

Madronich, S. 1987. Intercomparison of NO_2 photodissociation and UV radiometer measurements. *Atmos. Environ.* **21**, 569–578.

McKeen, S. A., Hsie, E.-Y., Trainer, M., Tallamraju, R. and Liu, S. C. 1991. A regional model of ozone budget in the eastern United States. *J. Geophys. Res.* **96**, 10 809–10 845.

McKeen, S. A., Mount, G., Eisele, F., Williams, E., Harder, J. et al. 1997. Photochemical modeling of hydroxyl and its relationship to other species during the tropospheric OH photochemistry experiment. *J. Geophys. Res.* **102**, 6467–6485.

Oltmans, S. J., Lefohn, A. S., Scheel, H. E., Harris, J. M., Levy, H. II et al. 1998. Trends of ozone in the troposphere. *Geophys. Res. Lett.* **25**, 139–142.

Pierce, T., Geron, C., Bender, L., Dennis, R., Tonnesen, D. et al. 1998. Influence of increased isoprene emissions on regional ozone modeling. *J. Geophys. Res.* **103**, 25 611–25 629.

Roselle, S. J., Pierce, T. E. and Schere, K. L. 1991. The sensitivity of regional ozone modeling to biogenic hydrocarbons. *J. Geophys. Res.* **96**, 7371–7394.

Roselle, S. J. and Schere, K. L. 1995. Modeled response of photochemical oxidants to systematic reductions in anthropogenic volatile organic compound and NOx emissions. *J. Geophys. Res.* **100**, 22 929–22 941.

Schere, K. L. and Wayland, R. A. 1989. *EPA Regional Oxidant Model (ROM 2.0): Evaluation on the 1980 NEROS Databases*. EPA-600/3–89-057. Environmental Protection Agency, Research Triangle Park, NC.

Shallcross, D. E. and Monks, P. S. 2000. New directions: a role for isoprene in biosphere-climate-chemistry feedbacks. *Atmos. Environ.* **34**, 1659–1660.

Sillman, S. 1995. The use of NOy, H_2O_2, and HNO_3 as indicator for the NOx-hydrocarbon sensitivity in urban locations. *J. Geophys. Res.* **100**, 14 175–14 188.

Sillman, S., Logan, J. A. and Wofsy, S. C. 1990. The sensitivity of ozone to nitrogen oxides and hydrocarbons in regional ozone episodes. *J. Geophys. Res.* **95**, 1837–1851.

Smolarkiewicz, P. K. 1983. A simple positive definite advection scheme with small implicit diffusion. *Mon. Weather Rev.* **11**, 479–486.

Streets, D. G., Bond, T. C., Carmichael, G. R., Fernandes, S. D., Fu, Q. et al. 2003. An inventory of gaseous and primary emissions in Asia in the year 2000. *J. Geophys. Res.* **108**(D21), 8809, doi:10.1029/2002JD003093.

Trainer, M., Williams, E. J., Parrish, D. D., Buhr, M. P., Allwine, E. J. et al. 1987. Models and observations of the impact of natural hydrocarbons on rural ozone. *Nature* **329**, 705–707.

Vincent, T. F. C. and Wang, T. 2001. Observational study of ozone pollution at a rural site in the Yangtze Delta of China. *Atmos. Environ.* **35**, 4947–4958.

Vogel, B., Riemer, N., Vogel, H. and Fiedler, F. 1999. Finds on NOy as an indicator for ozone sensitivity based on different numerical simulations. *J. Geophys. Res.* **104**, 3605–3620.

Wang, T. J., Lin, L. S., Li, Z. K. and Lam, K. S. 2000. A modeling study on acid rain and recommended emission control strategies in China. *Atmos. Environ.* **34**, 4467–4477.

Zhang, Y. H., Shao, K. S. and Tang, X. Y. 1998. The study of urban photochemical smog pollution in China. *Acta Sci. Nat. Universitatis Pekinensis* **34**, 392–400.

Zhang, M. G., Uno, I., Sugata, S., Wang, Z. F., Byun, D. et al. 2002. Numerical study of boundary layer ozone transport and photochemical production in East Asia in the wintertime. *Geophys. Res. Lett.* **29** (11), 1545, doi:10.1029/2001GL014368.